ACS APPLIED MATERIALS & INTERFACES

Research Article

Cite This: ACS Appl. Mater. Interfaces 2019, 11, 41109−41117

www.acsami.org

^{99m}Tc-, ^{90}Y-, and ^{177}Lu-Labeled Iron Oxide Nanoflowers Designed for Potential Use in Dual Magnetic Hyperthermia/Radionuclide Cancer Therapy and Diagnosis

Miloš Ognjanović,*[,†] Magdalena Radović,[†] Marija Mirković,[†] Željko Prijović,[†] Maria del Puerto Morales,[‡] Miran Čeh,[§] Sanja Vranješ-Đurić,[†] and Bratislav Antić[†]

[†]The Vinca Institute of Nuclear Sciences, University of Belgrade, Mike Petrovića Alasa 12-14, 11001 Belgrade, Serbia

[‡]Instituto de Ciencia de Materiales de Madrid, CSIC, Campus de Cantoblanco, 28049 Madrid, Spain

[§]Department for Nanostructured Materials, Jožef Štefan Institute, Jamova 39, 1000 Ljubljana, Slovenia

Supporting Information

ABSTRACT: Development of a complex based on iron oxide nanoparticles (IONPs) for diagnosis and dual magnetic hyperthermia/radionuclide cancer therapy accomplishing high yields of radiolabeling and great magnetic heat induction is still a challenge. We report here the synthesis of citric acid, poly(acrylic acid) (PAA) and poly(ethylene glycol) coated IONPs and their labeling with three radionuclides, namely, technetium (^{99m}Tc), yttrium (^{90}Y), and lutetium (^{177}Lu), aiming at potential use in cancer diagnosis and therapy. Polyol-synthesized IONPs are a flowerlike structure with 13.5 nm spherically shaped cores and 24.8 nm diameter. PAA-coated nanoparticles (PAA@IONP) showed the best characteristics such as easy radiolabeling with very high yields (>97.5%) with all three radionuclides, and excellent in vitro stabilities with less than 10% of radionuclides detaching after 24 h. Heating ability of PAA@IONP in an alternating external magnetic field showed intrinsic loss power value of 7.3 nH m^2/kg, which is one of higher reported values. Additionally, PAA@IONP itself presented no significant cytotoxicity to the CT-26 cancer cells, reaching IC50 at 60 μg/mL. However, under the external magnetic field, they show hyperthermia-mediated cells killing, which correlated with the magnetic field strength and time of exposure. Since PAA@IONP are easy to prepare, biocompatible, and with excellent magnetic heat induction, these nanoparticles radiolabeled with high-energy beta emitters ^{90}Y and ^{177}Lu have valuable potential as agent for dual magnetic hyperthermia/radionuclide therapy, while radiolabeled with ^{99m}Tc could be used in diagnostic imaging.

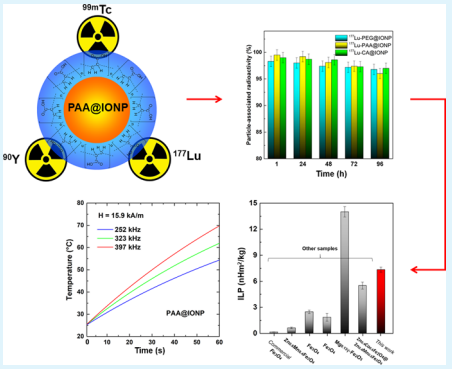

KEYWORDS: *magnetic nanoparticles, hyperthermia, radiolabeling, cytotoxicity, dual cancer therapy*

1. INTRODUCTION

Development of magnetic nanomaterials with new and exciting properties suitable for application in various fields of industry and medicine has been massively exploited during the last decades.[1−3] Recently, many studies on diagnostic and therapeutic use of iron-oxide based magnetic nanoparticles (IONPs) for various diseases including cancer are in progress.[4−6] Such IONPs may serve either as a contrast agent, carriers of radionuclides and drugs, mediators for magnetic hyperthermia therapy or combined hyperthermia and radionuclide therapy, etc.[8,9] Combining diagnostic and therapy approach into one, theranostic, researchers open new avenues for their further improvement.[7]

IONPs have been used as T2-MRI contrast agent for imaging purposes, while radiolabeled with ^{99m}Tc, due to their high imaging sensitivity, were proposed as gamma imaging agent for early and accurate diagnosis.[10−13] Moreover, IONPs radiolabeled with beta-emitting radionuclides yttrium (^{90}Y) and lutetium (^{177}Lu) can be potentially used in cancer radionuclide therapy.[13]

However, magnetic hyperthermia applied in cancer therapy is a process based on the harmful heat that magnetic nanoparticles produce under the oscillating magnetic field.[14] Despite frequent use, this method still encounters several problems, such as insufficient heat generated to harm surrounding tissue and short-range effect. Many synthesis methods of superparamagnetic nanoparticles were reported, including coprecipitation,[15] thermal decomposition in organic solvents,[16] microemulsion,[17] and microwave hydrothermal synthesis.[18] Unfortunately, very few of them allow the synthesis of nanoparticles with well-controlled particle size above the critical limit necessary for magnetic thermal blockage and usable for the application in magnetic hyperthermia.

Received: September 11, 2019
Accepted: October 14, 2019
Published: October 14, 2019

DOI: 10.1021/acsami.9b16428
ACS Appl. Mater. Interfaces 2019, 11, 41109−41117

With the aim to overcome some of the hyperthermia limitations, surface-modified improved IONPs with strong response to alternating-current (AC) magnetic field, suitable for radionuclide carriage and, thus, appropriate for multimodal use in diagnosis and therapy, were developed. Modification of nanoparticles' surface with active compounds or polymer shield particles from agglomeration and aggregation, enabling longer circulation time in blood and making possible their additional functionalization (i.e., binding of ligands, radionuclides, specific proteins, etc. on the surface of nanoparticles).[19]

The current study aimed to produce radiolabeled IONPs for potential use in diagnosis or combined hyperthermia/radionuclide cancer therapy. A modified polyol process was investigated for the synthesis of flowerlike IONPs with sufficient thermal properties where citric acid (CA), poly(acrylic acid) (PAA), and poly(ethylene glycol) (PEG) coatings were used for the efficient binding of different radionuclides (^{99m}Tc, ^{90}Y, and ^{177}Lu). Initial assessment of the microstructural and magnetic characteristics as well as behavior against cancer cells of radiolabeled IONP were studied thereafter as essential for the exploration of their potential for the theranostic applications.

2. MATERIALS AND METHODS

2.1. Materials. All chemicals were used as supplied and without any further purification. Iron(II) chloride tetrahydrate, iron(III) chloride hexahydrate, iron(III) nitrate nonahydrate, diethylene glycol (DEG), *N*-methyldiethanolamine (NMDEA), sodium hydroxide, nitric acid (HNO_3), CA, and PAA were purchased from Sigma-Aldrich. The poly(ethylene glycol) (average M_w 1000) was purchased from Merck. Technetium pertechnetate was eluted from Vinča's ^{99}Mo/^{99m}Tc generator, while yttrium chloride ($^{90}YCl_3$, 74.9 GBq/cm^3) and lutetium chloride ($^{177}LuCl_3$, 240.6 GBq/cm^3) were obtained from Polatom, Poland. In all experiments, ultrapure Milli-Q water was used (Millipore Co.).

2.2. Synthesis and Coatings of IONP. IONPs were prepared by the polyol process based on precipitation of iron salts with NaOH in NMDEA and DEG medium.[20] Briefly, 1.082 g of $FeCl_3{\cdot}6H_2O$ and 0.398 g of $FeCl_2{\cdot}4H_2O$ were added to a mixture of solvents containing 38.5 mL of NMDEA and 38.5 mL of DEG and stirred for 1 h. After the addition of 16 mM NaOH suspended in polyols the suspension was kept stirring for 3 h more. Solvothermal synthesis was performed in the suspension in autoclave cuvette kept at 220 °C for 12 h (oven Memmert UN55) followed by cooling of the system inside of the oven to room temperature (RT). The formed precipitate was separated magnetically and washed with an ethanol/ethyl acetate (50/50 v/v) solution. After that, standard protocol for acid treatment using 30 mL of 10% HNO_3 was used to reduce surface nanoparticle imperfections.[21] Then, the supernatant was discarded by magnetic separation, and 0.02 M $Fe(NO_3)_3$ and 20 mL of water was added to the mixture and stirred for 45 min at 80 °C. After they cooled to RT, the particles were dispersed in 20 mL of pure water and filtered through the 0.22 μm hydrophilic poly(ether sulfone) membrane. Finally, a portion of the sample was dried for 24 h at 60 °C for further use.

Coating of the synthesized nanoparticles was performed by the addition of previously determined amounts of CA (0.6 mM/g_{np}), PAA (0.6 mM/g_{np}), and PEG (5 mM/g_{np}) and sonication for 1 h at RT. Excess of unreacted CA, PAA, and PEG in solution was avoided by precisely dosing the amounts of surfactants that resulted in low amount of unreacted material, which is further eliminated by dialysis against deionized water during 24 h.[22] A stable suspension of coated iron oxide suspension at physiological pH was obtained. The coated samples were marked as CA@IONP, PAA@IONP, and PEG@IONP.

2.3. Characterization. The crystal structure was determined by X-ray powder diffraction (XRPD) measured on a high-resolution SmartLab X-ray diffractometer (Rigaku) operating at 40 kV and 30 mA and equipped with Cu Kα radiation (λ = 1.542 Å). The XRPD pattern was collected within 10−70° 2θ range with the following measuring conditions: divergent slit of 0.5 mm and speed of measurement 0.2°/min. The mean crystallite size (d_{XRPD}) was calculated by applying Scherrer's formula on the most intensive diffraction peaks. The particle size, morphology, and crystal structure of the synthesized nanoparticles were investigated by transmission electron microscopy (TEM) and selected area electron diffraction (SAED) analysis using transmission electron microscopes JEOL JEM-2100 and JEOL JEM-2100F UHR (Oxford, UK) operating at 200 keV. The TEM images were analyzed manually by ImageJ software.[23] Distribution and the average size of nanoparticles were estimated by measuring the largest diameter of at least 200 nanoparticles. Then, the obtained data were fitted to a log-normal function (eq 1)

$$y = y_0 + \frac{A}{\sqrt{2\pi\omega x}} \exp \frac{-\left[\ln \frac{x}{x_c}\right]^2}{2\omega^2} \quad (1)$$

to acquire the mean particle size and standard deviation (σ), which represents the absolute error of the measurement.

Magnetic measurements were performed using a Quantum Design MPMS 5XL magnetometer. The homogenized sample was packed in gelatin capsules (ca. 50 mg). Magnetization curves were measured at 300 and 5 K between −3988.5 and +3988.5 kA/m ($\pm T$). The saturation magnetization (M_s) was calculated by the eq 2 for H approaching ∞.[24]

$$M = M_s\left(1 - \frac{a}{H} - \frac{b}{H^2}\right) \quad (2)$$

After surface modification, zeta potentials of coated IONPs were measured on water colloidal dispersions at 25.0 ± 0.1 °C in Nano ZS90 device (Malvern). The zeta potentials of PAA@IONP were recorded at pH ≈ 6−7 and 0.01 M ionic strength. Afterward, zeta potential curves were fitted to a Boltzmann sigmoidal function (eq 3):

$$y = \frac{A_1 - A_2}{1 + e^{(x - x_0)/dx}} + A_2 \quad (3)$$

Specific absorption rates (SAR) were determined by calorimetric measurements on commercial AC apparatus (model DM 100 nB nanoScale Biomagnetic). Kinetic curves were recorded under a magnetic field of 15.9 kA/m and three different frequencies in the range of 252−397 kHz. Measurements were conducted during 60 s in water colloidal dispersions of the IONP concentration of 5 mg/mL. For the determination of SAR values, an increase of the temperature was monitored by an optical fiber system immersed into 1 mL of sample. The temperature of suspension was maintained below 65 °C to decrease evaporation, which could destabilize colloidal suspension and reduce the measurement's precision. The SAR values were determined by linear fitting of calorimetric curves in the first 20 s of measurements $(dT/dt)_0$ using a corrected slope method to amend any linear losses[25] using eq 4

$$\text{SAR (W/g)} = c_{NP} + \frac{\rho_1}{\rho_{NP}} \times c_1 \times \left(\frac{dT}{dt}\right)_{max} \quad (4)$$

where C_{NP} is given as specific heat of the nanoparticles (J/(kg·K)), ρ_{NP} as density of IONP in the colloid (kg/m^3), ρ_1 as density of the dispersing agent (kg/m^3), and $(dT/dt)_{max}$ as maximum gradient of the temperature of the calorimetric curve (K/s). SAR is measured as watts per gram of nanoparticles.

Intrinsic loss power (ILP), which can be used for the characterization of the magnetic nanoparticles' intrinsic efficiency to absorb power, was calculated from eq 5

$$\text{ILP (nH m}^2\text{/kg)} = \frac{\text{SAR}}{H^2 f} \quad (5)$$

DOI: 10.1021/acsami.9b16428
ACS Appl. Mater. Interfaces 2019, 11, 41109−41117

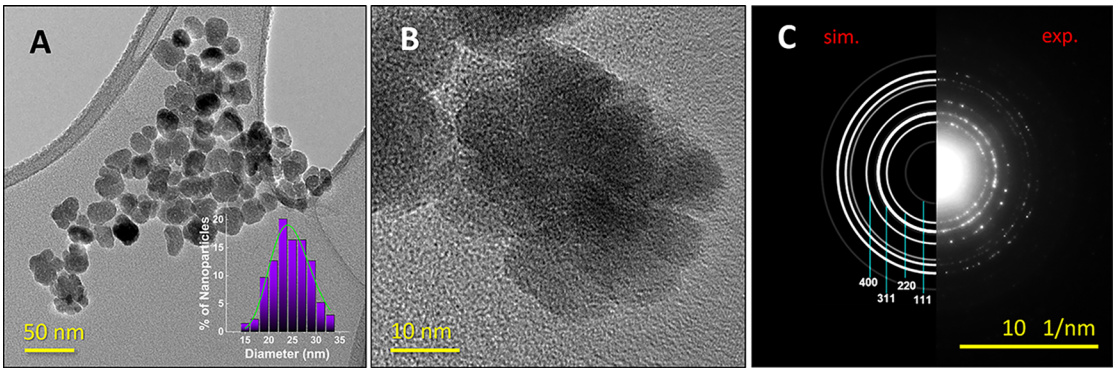

Figure 1. Morphological and microstructural properties of IONP. (A) TEM bright-field image with log-normal size distribution (inset). (B) Nanoflower TEM image (see text) and (C) SAED pattern, experimental and simulated according to $Y_{0.15}Fe_{2.85}O_4$: PDF No. 04-014-1397.

where H_0 is an intensity of the applied magnetic field (A/m), and f is the frequency of applied field (Hz). The ILP value of a magnetic colloid is independent of the equipment used.

2.4. Radiolabeling of Coated IONP. *^{99m}Tc Labeling.* The CA, PAA, and PEG-coated IONP (5 mg/mL) were radiolabeled by ^{99m}Tc using $SnCl_2$ for reduction of $^{99m}Tc^{7+}$. Reactions were performed by simultaneous addition of 0.1 mL of $Na^{99m}TcO_4$ (18.5 MBq) and 0.04 mL of $SnCl_2$ solution (2.5 mg/mL in 0.5 M HCl) to the suspensions of 0.02 mL of surface-modified IONP in 1 mL of sterile water. After adjustment of the pH to 6, the reaction mixture was gently stirred at RT for 30 and 60 min.

Two radiochromatographies on silica gel (instant thin-layer chromatography−silica gel (ITLC-SG)), one with acetone and another with a mixture of pyridine/acetic acid/water (3:5:1.5 v/v)[26] were used to determine the radiolabeling yield of the ^{99m}Tc-labeled coated IONP. Dose calibrator (CRC-15, Capintec) and gamma counter (Wizard 2480, PerkinElmer) were employed to measure the radioactivity of all samples.

^{90}Y Labeling. ^{90}Y labeling was performed by incubation (for 30 and 60 min) of 0.1 mL of suspension (pH 4−5) of coated IONP (5 mg/mL) with 0.006 mL of $^{90}YCl_3$ (185 MBq) in two experiments (at 25 and 60 °C). ITLC method, on silica gel (SG) sheets with saline as the mobile phase, was used to determine the radiolabeling yield of ^{90}Y-IONP. With this method the unbound $^{90}Y^{3+}$ migrated with the front (R_f = 0.9−1.0), while radiolabeled particles did not migrate (R_f = 0.0−0.1). Yttrium-90 as a pure β-emitter was detected by "bremsstrahlung" effect.[27]

^{177}Lu Labeling. An appropriate volume of $^{177}LuCl_3$ solution in 0.04 M HCl (185 MBq) was taken in a vial containing 0.1 mL of coated IONP (5 mg/mL) at pH 5−6 and incubated for either 30 or 60 min at RT. The radiolabeling yield determined by ITLC method (the same as for the ^{90}Y-IONP) showed that $^{177}Lu^{3+}$ migrated with the solvent front (R_f = 0.8−0.9), while the ^{177}Lu-labeled coated IONP did not migrate (R_f = 0.0−0.1).

2.5. In Vitro Stability of the Radiolabeled Coated IONP. The in vitro stability of CA, PAA, and PEG-coated IONP labeled with ^{99m}Tc, ^{90}Y, and ^{177}Lu was tested in saline and human serum (HS, Blood Transfusion Institute, Serbia) after incubation at 37 °C during 24 h for ^{99m}Tc-labeled coated IONP, and during periods of 72 and 96 h for ^{90}Y- and ^{177}Lu-labeled coated IONP, respectively. At different times after radiolabeling, the activity of samples was analyzed by ITLC-SG using the solvent systems specified above for each radionuclide.

2.6. Cytotoxicity of IONP in Vitro. For cytotoxicity studies and effect of oscillating magnetic field-generated hyperthermia on cancer cells, CT-26 mouse colon carcinoma cells were cultured in monolayer in tissue culture dishes in RPMI medium supplemented with 10% fetal bovine serum (FBS), 100 IU/mL penicillin, and 100 ug/mL streptomycin, in a humidified atmosphere with 5% CO_2 at 37 °C. When 80% confluent, the cells were harvested after trypsin/ethylenediaminetetraacetic acid (EDTA) solution exposure and washed. Upon resuspension in complete medium and counting in Neubauer chamber, concentration of the cells is adjusted to 1×10^5 cells/mL, and 0.1 mL (1×10^4 cells/well) was dispensed into wells of 96-well plates. The attached cells were exposed to IONP for 24 h in the incubator. Afterward, the cells were washed to remove the IONP; the medium was replaced with fresh one and left for another 24 h before quantification by 3-(4,5-dimethylthiazol-2-yl)-2,5-diphenyltetrazolium bromide (MTT) assay. Briefly, after replacement of the old medium by 0.1 mL of fresh medium containing 0.5 mg/mL MTT and incubation for 4 h in the dark, the medium was carefully aspirated. Formed dye was dissolved by 0.1 mL of dimethyl sulfoxide (DMSO) with shaking for 30 min, and the color was quantitated by absorbance measurement at 560 nm using 96-well plate reader (Molecular Devices Spectramax 250).

2.7. Hyperthermia Effect of IONPs on CT-26 Cancer Cells in Vitro. To investigate the cytotoxicity of IONP in presence and absence of magnetic field on cancer cells, 1×10^4 cells/well of CT-26 cells were cultured overnight in 96-well plates to allow the cells to attach. The media was replaced with 0.1 mL of a fresh medium containing serial twofold dilution of IONP, starting with 1 mg/mL in duplicates. After 15 min, the plates were exposed to the alternating magnetic field at three different frequencies (82, 100, and 116 kHz) for 5, 15, and 30 min at field strength of H = 7.95 kA/m. After the exposure, the wells were washed to remove the IONP, fresh medium was added, and the cells left to recover for 24 h. Number of surviving cells was determined by MTT assay as described above.

3. RESULTS AND DISCUSSION

Aiming to produce IONPs with excellent heating abilities, yet easy to be radiolabeled, making them suitable for hyperthermia/radiotherapy or diagnosis of cancers, we used a method of synthesis that allows generation of IONPs of suitable, well-controlled size in form of nanoflowers. The iron oxide nanoparticles were synthesized via the polyol method as described elsewhere[20] due to superior properties compared to other methods of synthesis. The obtained IONPs were coated to shield them from aggregation, still improving biocompatibility and allowing easy radiolabeling. These IONPs were radiolabeled with different radionuclides and characterized for their physical and chemical properties and in vitro stability. The cytotoxicity toward CT-26 cancer cells in vitro and magnetic hyperthermia efficiency by exposure to various magnetic field parameters of IONP were investigated. Altogether, we developed a robust and practical system for generation of nanoflower-like radiolabeled IONPs with great properties for use in cancer diagnosis and therapy. The detailed results are described below.

3.1. Morphology, Microstructure, and Magnetization Properties of IONP. Morphology and size of IONP were determined by TEM. The representative TEM micrographs in

DOI: 10.1021/acsami.9b16428
ACS Appl. Mater. Interfaces 2019, 11, 41109−41117

Figure 1A show that nanoparticles, ~13.5 (±1.2) nm in size, form small agglomerates with sizes that fit to a log-normal distribution giving a mean average diameter of 24.8 (±4.4) nm and a polydispersity (σ) of 18% (inset of Figure 1A). The image displayed in Figure 1B presents the agglomeration of some individual particles to nanoflower structure.[20,28] The individual nanoparticle's shape is an intermediate between spherical and rounded cubes. SAED was analyzed by a comparison between simulated[29] and experimental data (Figure 1C). It indicates that IONPs crystallize to spinel structure type, space group $Fd\bar{3}m$, matching the most intensive diffraction peaks with simulated diffraction data. However, at the nanoscale, it is very difficult to observe a difference between magnetite and maghemite by diffraction techniques.

The IONPs were further characterized by XRPD technique. The representative XRPD pattern is shown in Figure 2A. The

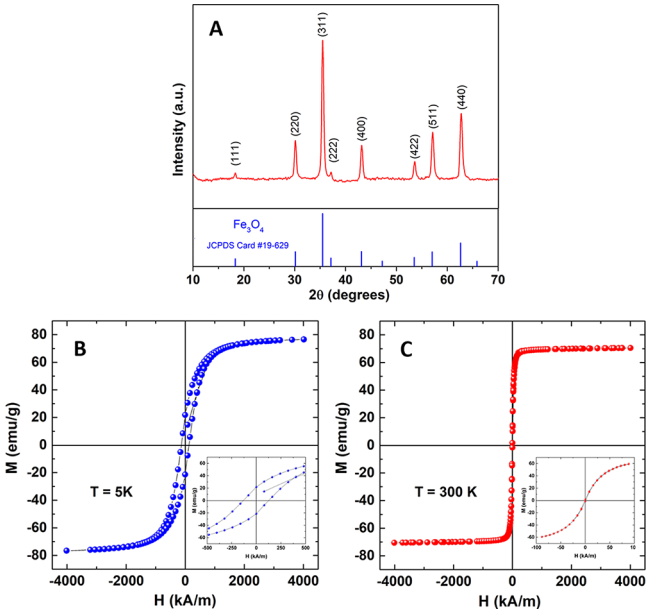

Figure 2. (A) XRD pattern obtained by the Cu Kα source-equipped diffractometer. Magnetization vs magnetic field curves of IONP at (B) 5 and (C) 300 K.

reflections of IONP are present at approximately identical 2θ angle and intensity as those of Fe_3O_4; hence, they could be attributed to the $Fd\bar{3}m$ space group of the cubic structure (No. 227). This confirms that the sample crystallizes in the spinel structure group (JCPDS Card No. 19-629). Nevertheless, a more detailed XRPD analysis of a similar synthesis method suggested a maghemite structure (γ-Fe_2O_3).[30] On the basis of XRPD and SAED results, synthesized nanoparticles are most likely to be a combination of both crystal phases (maghemite and magnetite). The lattice parameter of the IONP was determined to be a = 8.3823(3) Å.

To further investigate the magnetization properties of IONP, several different methods were performed. The isothermal magnetization measurements were done at 5 and 300 K (RT) in the field range up to 3988.5 kA/m. The insets in Figure 2B,C represent the hysteresis loops in the low-field regime. The saturation magnetization (M_s) values of nanoparticles at 5 and 300 K are ~77 and 70.5 emu/g, respectively, which is in agreement with similarly shaped IONP.[30] The magnetization curve at Figure 2C goes through the origin of magnetization graph, suggesting that synthesized IONPs are superparamagnetic at RT, while the coercivity is present at 5 K with value 231.3 kA/m (Figure 2B).

3.2. Radiolabeling and in Vitro Stability Studies of Coated IONP. With the aim to find simple, fast, and reliable methods applicable for the binding of different radionuclides to IONPs with various coatings, a study was done with CA, PAA, and PEG-coated IONPs and radionuclides ^{99m}Tc, ^{90}Y, and ^{177}Lu. With radionuclide's ability to form complexes with different groups of surface coatings of IONP, the indirect radiolabeling method for all three radionuclides and mild conditions were first investigated.[31−33] The same method for particles' radiolabeling may be used not only for the monitoring of IONP in experimental condition in vitro and in vivo but also for radiodiagnosis or radiotherapy.[34,35] Besides, theranostic approach may be easily achieved with the same nanoparticles, while chelator enables substitution of gamma-emitting radionuclides used for diagnostic with a therapeutic radionuclide. ^{99m}Tc labeling was performed with the addition of an acidic $SnCl_2$ solution allowing reduction of $^{99m}Tc^{7+}$ to lower oxidation states necessary for the formation of ^{99m}Tc complexes. Radiolabeling yields of ^{99m}Tc-PAA@IONP and ^{99m}Tc-CA@IONP, detected by ITLC-SG, were very high (97.5% and 98.5%, respectively), while the radiolabeling yield of ^{99m}Tc-PEG@IONP was 69.2%. Radiolabeling was completed very fast, for 30 min, at mild conditions (room temperature and neutral pH), while increasing the reaction time to 60 min insignificantly changed the radiolabeling yield (Table 1). ^{99m}Tc-Labeled nanoparticles may be used in

Table 1. Radiolabelling Yields of Coated IONP for Different Labelling Conditions with ^{99m}Tc, ^{90}Y, and ^{177}Lu

	radiolabeling yield (%)					
	with ^{99m}Tc		with ^{90}Y		with ^{177}Lu	
	T = 25 °C		T = 25 °C		T = 25 °C	
IONP	30 min	60 min	30 min	60 min	30 min	60 min
PEG@IONP	69.2	68.3	99.8	99.4	98.4	98.5
PAA@IONP	97.5	97.1	99.5	99.5	99.7	99.6
CA@IONP	98.5	98.4	99.2	99.3	99.3	99.1

diagnosis, while the same radiolabeling method may be efficiently used for the radiolabeling of coated IONPs with ^{188}Re for the therapeutical use because of the similar chemical properties of these radionuclides.[36]

High radiolabeling yields (>99%) were found for all three coated IONP radiolabeled with ^{90}Y, after incubation for 30 min at 25 °C. The radiolabeling of coated IONP with ^{177}Lu was also performed at high yields (>98%) at 25 °C after 30 min, and prolonged reaction time to 60 min did not have significant impact on the radiolabeling yield. These results could be explained by the binding of positively charged radionuclides through negatively charged carboxylate groups present on PAA@IONP and CA@IONP and hydroxyl groups present on PEG@IONP surface. PEG provides a hydrophilic layer that makes IONPs dispersible in water and internanoparticle steric repulsion preventing aggregation. Unfortunately, hydroxyl groups from the PEG surface were not able to bind ^{99m}Tc in high yield, and therefore additional chelator with high affinity toward ^{99m}Tc is necessary.

The above labeling approach with surface coatings is easy and fast to perform and leads to the formation of complexes that are stable in aqueous solution. PAA seems to be especially

DOI: 10.1021/acsami.9b16428
ACS Appl. Mater. Interfaces 2019, 11, 41109−41117

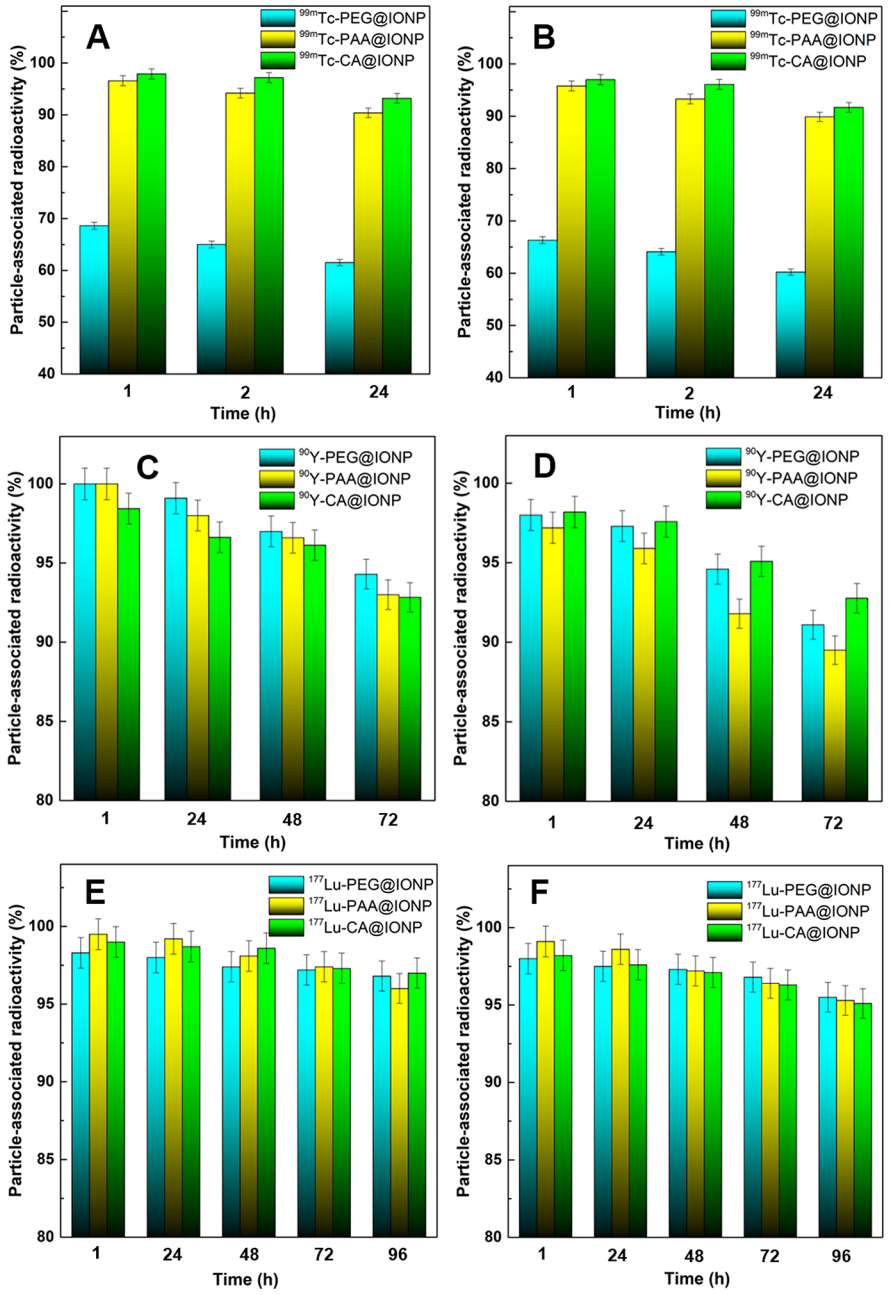

Figure 3. In vitro stability of ^{99m}Tc-PEG@IONP, ^{99m}Tc-PAA@IONP, and ^{99m}Tc-CA@IONP in (A) saline and (B) human serum after incubation at 37 °C over 24 h; ^{90}Y-PEG@IONP, ^{90}Y-PAA@IONP, and CA@IONP in (C) saline and (D) human serum after incubation at 37 °C over 72 h and ^{177}Lu-PEG@IONP, ^{177}Lu-PAA@IONP, and ^{177}Lu-CA@IONP in (E) saline and (F) human serum after incubation at 37 °C over 96 h.

convenient for radiolabeling with different metallic radionuclides because of the variety of available groups ready for binding. CA has very high binding efficacy, especially for ^{90}Y and ^{177}Lu; therefore, special attention should be applied on the complete elimination of unbound ligands from the IONP suspension, since it may bind radionuclides attended for the radiolabeling of coated IONP.

Radiolabeled coated IONPs were left in saline or human serum for in vitro stability studies, and at several time points (1, 2, and 24 h) they were analyzed by ITLC. ^{99m}Tc-PEG@IONP with lower but acceptable radiolabeling yield was in vitro studied after purification, using simple magnetic decantation as follows: the supernatant with unbound radionuclide was withdrawn, while precipitate with IONP was washed with deionized water to remove free radionuclides. All three ^{99m}Tc-coated IONPs were very stable in saline, showing less than 10% of detached ^{99m}Tc after 24 h, with the highest rate of detaching in the first hour (Figure 3A,B). Similar stability was achieved in human serum. In vitro stability of ^{90}Y-coated IONP was very high both in saline as well as in human serum with less than 8% of free ^{90}Y after 72 h (Figure 3C,D). The in vitro stability of ^{177}Lu-CA, PAA, and PEG@IONP in the same physiological media retained more than 95% even after 96 h and, hence, could be considered remarkably stable (Figure 3E,F).

After physicochemical characterization of radiolabeled IONP, PAA@IONP was selected as the best candidate and therefore was further used for zeta potential measurements and

DOI: 10.1021/acsami.9b16428
ACS Appl. Mater. Interfaces 2019, 11, 41109−41117

magnetic hyperthermia studies. Besides similar radiolabeling yield and in vitro stability, the main advantage of PAA@IONP is that there is no need for the additional purification after coating resulting in simple and fast radiolabeling.

3.3. Colloidal Properties of PAA@IONP. Well-established method for the surface modification of IONP is important to prevent decrease of AC-heating dissipation caused by thickness of coating or by aggregation of nanoparticles caused by the increase of particle volume. The measured zeta potential curves for uncoated and PAA-stabilized IONP are shown in Figure 4A. The successful

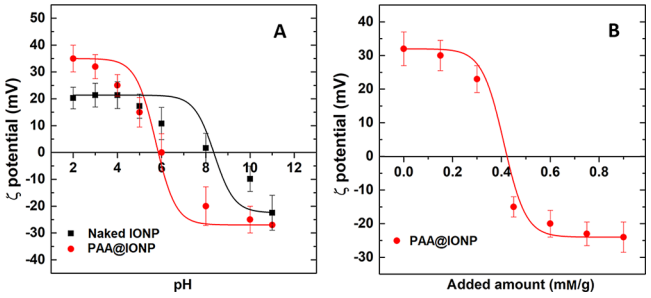

Figure 4. Effect of (A) pH on zeta potential of PAA@IONP and (B) added amount of PAA. Zeta potential curves are fitted to a Boltzmann sigmoidal function.

PAA coating of IONP with PAA, confirmed by the change of the isoelectric point (zero zeta potential) to lower pH values and by decrease of the surface charge from 14 to −26 mV at pH 7.5, improves the stability of IONP by electrostatic repulsion. The addition of carboxylic group-rich compound to the IONP dispersions at pH ≈ 6.5 and 0.01 M ionic strength had an obvious effect on the zeta potential of the IONP, as displayed in Figure 4B. The negatively charged polyacids neutralize the initial positive charges of the IONP at physiological pH during the adsorption of the negatively charged $-COO^-$ groups; hence, the addition of 0.4 mM/g of PAA resulted in a neutralization of charge (reducing the value of zeta potential to zero). Further adsorption of the negatively charged $-COO^-$ groups causes reversal in particle charge, reaching the minimum of electrokinetic potential at ∼0.6 mM/g of IONP.[22]

3.4. Cytotoxicity Study. Concentrations below 10 μg/mL IONP were nontoxic to the CT-26 mouse colon cancer cells (Figure S1A). Higher doses, however, expressed significant cytotoxicity, reaching IC50 at 60 μg/mL. Such a high concentration is unlikely to be achieved in in vivo experiments, so we may state that obtained IONP are nontoxic at physiologically achievable levels. Observation of the IONP over cells under a microscope revealed the accumulation of the IONP at the cells, probably contributing to the observed toxicity (Figure S1B,C).

3.5. Magnetic Hyperthermia Efficiency of PAA@IONP. Magnetic hyperthermia efficiency of PAA@IONP was determined as the temperature increase of aqueous dispersions of PAA@IONP over time under the influence of the external alternating magnetic field (Figure 5). The heating effect of PAA@IONP was measured in water at constant magnetic field H = 15.9 kA/m, while the resonant frequency was varied (Figure 5A), having in mind $H{\cdot}f$ product limitations.[37] To avoid potential local heating and undesirable damage in nonmagnetic tissues under AC magnetic field,[38] Brezovich proposed that product of field strength and frequency should be limited to a maximum of field-frequency product ($H{\cdot}f$) 4.85 × 10^8 A·m^{-1}·s^{-1} (Atkinson−Brezovich limit).[37] This limitation depends on application zone in the body and is not applicable in medical practice; hence, Hergt et al. suggested a less strict criterium: $H{\cdot}f \leq 5 \times 10^9$ A·m^{-1}·s^{-1}.[39] In the course of experiments presented in this study, the maximum of $H{\cdot}f$ product was 4.5 × 10^9 A·m^{-1}·s^{-1} (at 252 kHz and 15.9 kA/m), which is tolerable and within the Hergt's criterion. The higher applied frequencies (323 and 397 kHz) were used just for heating comparison and by comparing ILP for confirmation of particles' colloidal stability.

To quantitatively evaluate the intrinsic heating abilities and heat induction of material under the AC magnetic field, the ILP values of synthesized nanoparticles were determined from the SAR values (Figure 5B). The calculated ILP were approximately the same and equal to 7.3 (±0.2) nH m^2/kg independently on the applied frequency, suggesting that the IONP suspension is stable at any field's frequencies and

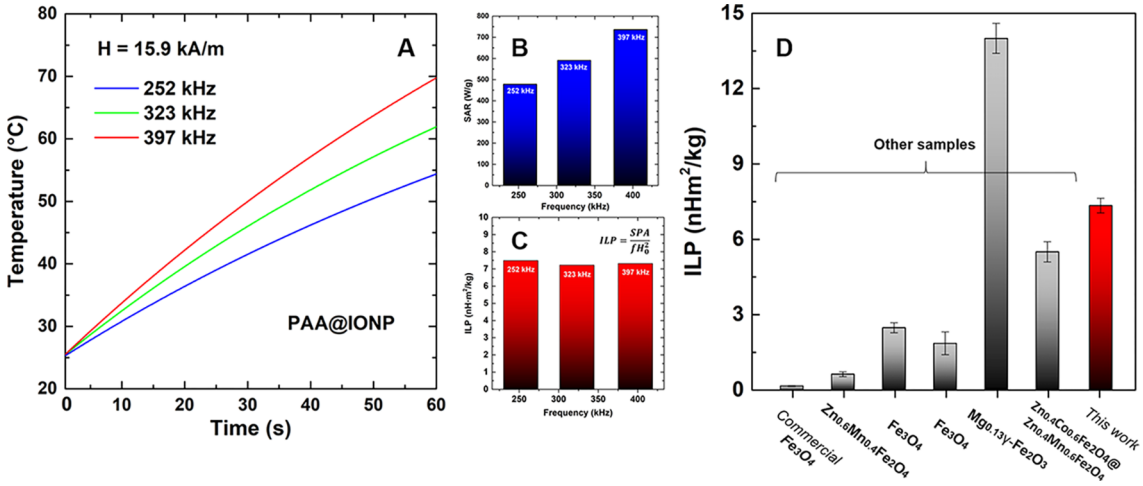

Figure 5. Magnetic hyperthermia measurements. (A) Time-dependent temperature curves obtained under a magnetic field of 15.9 kAm^{-1} and various frequencies. (B) Calculated SAR values. (C) Calculated ILP values and (D) comparison of ILP value of our developed IONP to other previously reported superparamagnetic nanoparticles.

DOI: 10.1021/acsami.9b16428
ACS Appl. Mater. Interfaces 2019, 11, 41109−41117

Table 2. Reported SAR and ILP Values of Various Superparamagnetic Nanoparticles

material	size d (nm)	frequency f (kHz)	amplitude H_0 (kA/m)	SAR (W/g)	ILP (nH m^2/kg)	ref
Fe_3O_4 (Feridex)	15	500	37.70	115	0.16	40
$Zn_{0.6}Mn_{0.4}F_2O_4$	15	500	37.70	432	0.63	41
Fe_3O_4	10	300	15	168	2.48	44
Fe_3O_4	14	400	24.5	447	1.86	45
$Mg_{0.13}\gamma$-Fe_2O_3	7	110	11.14	201	14.0	41
$Zn_{0.4}Co_{0.6}Fe_2O_4$@$Zn_{0.4}Mn_{0.6}Fe_2O_4$	15	500	37.70	3886	5.5	46
polyol IONP	core size 14	252	15.95	478	7.3	present study

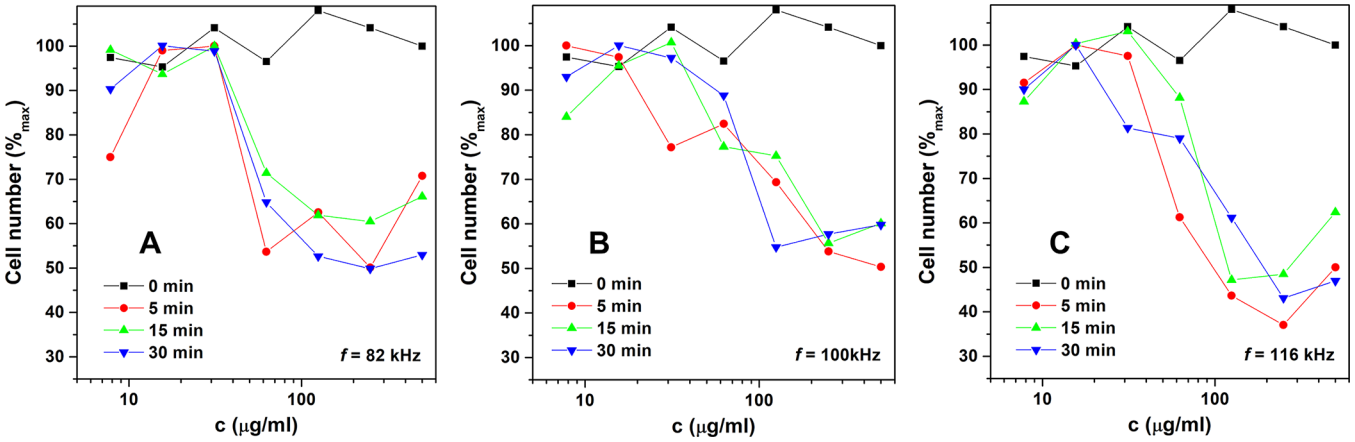

Figure 6. IONP-mediated hyperthermia cytotoxicity to CT-26 cells for different time period (A) at frequency of 82; (B) 100; and (C) 116 kHz at H = 7.95 kA/m.

amplitude, without the formation of chains or aggregates (Figure 5C).

The obtained ILP of PAA@IONP superparamagnetic nanoparticles is significantly (more than 11 times) higher in comparison to the ILP of some other core/shell nanoparticles[40] and almost 45 times higher compared to commercially available IONP (Feridex) (Figure 5D). According to the results published by Jang et al., there has been only one material containing Mg incorporated into γ-structure, with higher ILP values, that is ∼14 nHm^2/kg.[41] In this work, the extraordinary heating abilities of the magnetite nanoparticle suspension were probably due to specific particle organization and agglomeration of individual cores, their size of ∼14 nm just above the critical minimal limit necessary for magnetic thermal blockage and their combined interaction inside single nanoflower, resulting in high heat induction in AC magnetic field.[20,42,43] A comparison of the characteristics of various superparamagnetic nanoparticles is given in Table 2. Note that this correlation cannot be perfect due to the use of different equipment and measurement conditions and should be regarded just as an approximate guideline.

3.6. The Effect of Magnetic Hyperthermia on CT-26 Cancer Cells in Vitro. To evaluate the effect of oscillating magnetic field generated, IONP-mediated hyperthermia on cancer cells, CT-26 cells were subjected to the AC magnetic field of 7.95 kA/m, by increasing the frequency from 82 to 100 and 116 kHz and scaling the exposure time from 5 to 30 min (Figure 6). The increase of the magnetic field frequency indeed had more pronounced killing effect on the cells as well as the increase of exposure time, with the maximal effect observed at 116 kHz after 30 min. Further increase of the field frequency and exposure duration probably can produce even higher end-result. The effect of different frequencies for 30 min at H = 7.95 kA/m on CT-26 cancer cells with 1 mg/mL IONP was shown in Figure S2, while the effect of AC magnetic field on CT-26 without loaded IONP was displayed in Figure S3. The similar effect of hyperthermia against CT-26 cells with magnetic liposomes loaded with doxorubicin and glucose-coated IONP has been reported recently.[47,48]

4. SUMMARY

The polyol synthesized flowerlike IONPs were stabilized with three biocompatible compounds, namely, CA, PAA, and PEG. These coatings, among other purposes, prevent aggregation of IONP and increase biocompatibility and binding potential for different drugs. Indirect radiolabeling with radionuclides ^{90}Y, ^{177}Lu, and ^{99m}Tc via negative groups of coatings CA, PAA, and PEG was an adequate approach and enabled high radiolabeling yield. Among the tested samples, PAA@IONP had the best labeling yields (>97.5%) and in vitro stabilities with less than 10% of radionuclides detaching from nanoparticle surface in 24 h, so it was further tested as heating agent for magnetic hyperthermia in water and in vitro on CT-26 tumor cells, showing remarkable results. Outstanding heat performance with one of the highest reported ILP values for magnetite of 7.3 nHm^2/kg was obtained, enough to cause significant effect against cells exposed. High specific power absorption was probably a consequence of the specific organization and agglomeration of individual cores inside each particle, which is in good agreement with other results. On the basis of the presented results, PAA-coated nanoparticles, due to their excellent physicochemical and biological characteristics, most importantly high heat performance and high radiolabeling yields with different radionuclides, deserve further in vivo studies to investigate their potential as theranostic agent.

DOI: 10.1021/acsami.9b16428
ACS Appl. Mater. Interfaces 2019, 11, 41109−41117

■ ASSOCIATED CONTENT

Supporting Information

The Supporting Information is available free of charge on the ACS Publications website at DOI: 10.1021/acsami.9b16428.

Cytotoxicity of NPs to CT-26 cells after 24 h of exposure; the hyperthermia effect of different frequencies of oscillating magnetic field for 30 min at H = 7.95 kA/m on CT-26 with 1 mg/mL NPs; the effect of oscillating magnetic field on CT-26 without load of NPs at different frequencies (PDF)

■ AUTHOR INFORMATION

Corresponding Author

*E-mail: miloso@vin.bg.ac.rs.

ORCID

Miloš Ognjanović: 0000-0003-2889-4416

Maria del Puerto Morales: 0000-0002-7290-7029

Notes

The authors declare no competing financial interest.

■ ACKNOWLEDGMENTS

The authors gratefully acknowledge the support provided by the Eureka Project (E!9982) and Project No. III45015 funded by the Serbian Ministry of Education, Science and Technological Development, EU funded project FP7-EraChairs-MagBioVin (Grant No. 621375) and by the Spanish Ministerio de Ciencia, Innovación y Universidades (MAT2017-88148-R).

■ REFERENCES

(1) Jain, T. K.; Richey, J.; Strand, M.; Leslie-Pelecky, D. L.; Flask, C. A.; Labhasetwar, V. Magnetic nanoparticles with dual functional properties: drug delivery and magnetic resonance imaging. *Biomaterials* **2008**, *29*, 4012−4021.

(2) Tartaj, P.; Morales, M. P.; Veintemillas-Verdaguer, S.; González-Carreño, T.; Serna, C. J. The preparation of magnetic nanoparticles for applications in biomedicine. *J. Phys. D: Appl. Phys.* **2003**, *36*, R182.

(3) Stark, W. J.; Stoessel, P. R.; Wohlleben, W.; Hafner, A. Industrial applications of nanoparticles. *Chem. Soc. Rev.* **2015**, *44*, 5793−5805.

(4) Shao, H.; Min, C.; Issadore, D.; Liong, M.; Yoon, T.-J.; Weissleder, R.; Lee, H. Magnetic nanoparticles and microNMR for diagnostic applications. *Theranostics* **2012**, *2*, 55.

(5) Rümenapp, C.; Gleich, B.; Haase, A. Magnetic nanoparticles in magnetic resonance imaging and diagnostics. *Pharm. Res.* **2012**, *29*, 1165−1179.

(6) Goya, G. F.; Grazu, V.; Ibarra, M. R. Magnetic nanoparticles for cancer therapy. *Curr. Nanosci.* **2008**, *4*, 1−16.

(7) Singh, A.; Sahoo, S. K. Magnetic nanoparticles: a novel platform for cancer theranostics. *Drug Discovery Today* **2014**, *19*, 474−481.

(8) Johannsen, M.; Thiesen, B.; Wust, P.; Jordan, A. Magnetic nanoparticle hyperthermia for prostate cancer. *Int. J. Hyperthermia* **2010**, *26*, 790−795.

(9) Maier-Hauff, K.; Rothe, R.; Scholz, R.; Gneveckow, U.; Wust, P.; Thiesen, B.; Feussner, A.; von Deimling, A.; Waldoefner, N.; Felix, R.; et al. Intracranial thermotherapy using magnetic nanoparticles combined with external beam radiotherapy: results of a feasibility study on patients with glioblastoma multiforme. *J. Neuro-Oncol.* **2007**, *81*, 53−60.

(10) Kang, T.; Li, F.; Baik, S.; Shao, W.; Ling, D.; Hyeon, T. Surface design of magnetic nanoparticles for stimuli-responsive cancer imaging and therapy. *Biomaterials* **2017**, *136*, 98−114.

(11) de Barros, A. B.; Tsourkas, A.; Saboury, B.; Cardoso, V. N.; Alavi, A. Emerging role of radiolabeled nanoparticles as an effective diagnostic technique. *EJNMMI Res.* **2012**, *2*, 39.

(12) Madru, R.; Kjellman, P.; Olsson, F.; Wingårdh, K.; Ingvar, C.; Ståhlberg, F.; Olsrud, J.; Lätt, J.; Fredriksson, S.; Knutsson, L.; et al. ^{99m}Tc-labeled superparamagnetic iron oxide nanoparticles for multimodality SPECT/MRI of sentinel lymph nodes. *J. Nucl. Med.* **2012**, *53*, 459−463.

(13) Radović, M.; Mirković, M.; Perić, M.; Janković, D.; Vukadinović, A.; Stanković, D.; Petrović, Đ.; Bošković, M.; Antić, B.; Marković, M.; Vranješ-Đurić, S. Design and preparation of 90Y-labeled imidodiphosphate- and inositol hexaphosphate-coated magnetic nanoparticles for possible medical applications. *J. Mater. Chem. B* **2017**, *5*, 8738−8747.

(14) Pankhurst, Q. A.; Connolly, J.; Jones, S. K.; Dobson, J. J. Applications of magnetic nanoparticles in biomedicine. *J. Phys. D: Appl. Phys.* **2003**, *36*, R167.

(15) Massart, R. Preparation of aqueous magnetic liquids in alkaline and acidic media. *IEEE Trans. Magn.* **1981**, *17*, 1247−1248.

(16) Roca, A. G.; Morales, M. P.; O'Grady, K.; Serna, C. J. Structural and magnetic properties of uniform magnetite nanoparticles prepared by high temperature decomposition of organic precursors. *Nanotechnology* **2006**, *17*, 2783.

(17) Mathew, D. S.; Juang, R.-S. An overview of the structure and magnetism of spinel ferrite nanoparticles and their synthesis in microemulsions. *Chem. Eng. J.* **2007**, *129*, 51−65.

(18) Ognjanović, M.; Dojčinović, B.; Fabián, M.; Stanković, D. M.; Mariano, J. F. M. L.; Antić, B. Microwave assisted hydrothermal synthesis of $(Fe,Co)_3O_4$ nanoparticles in the presence of surfactants and effects of Co/Fe ratio on microstructure and magnetism. *Ceram. Int.* **2018**, *44*, 13967−13972.

(19) Albanese, A.; Tang, P. S.; Chan, W. C. W. The effect of nanoparticle size, shape, and surface chemistry on biological systems. *Annu. Rev. Biomed. Eng.* **2012**, *14*, 1−16.

(20) Hugounenq, P.; Levy, M.; Alloyeau, D.; Lartigue, L.; Dubois, E.; Cabuil, V.; Ricolleau, C.; Roux, S.; Wilhelm, C.; Gazeau, F.; et al. Iron oxide monocrystalline nanoflowers for highly efficient magnetic hyperthermia. *J. Phys. Chem. C* **2012**, *116*, 15702−15712.

(21) Costo, R.; Bello, V.; Robic, C.; Port, M.; Marco, J. F.; Puerto Morales, M.; Veintemillas-Verdaguer, S. Ultrasmall iron oxide nanoparticles for biomedical applications: improving the colloidal and magnetic properties. *Langmuir* **2012**, *28*, 178−185.

(22) Tombácz, E.; Tóth, I. Y.; Nesztor, D.; Illés, E.; Hajdú, A.; Szekeres, M.; Vékás, L. Adsorption of organic acids on magnetite nanoparticles, pH-dependent colloidal stability and salt tolerance. *Colloids Surf., A* **2013**, *435*, 91−96.

(23) Schneider, C. A.; Rasband, W. S.; Eliceiri, K. W. NIH Image to ImageJ: 25 years of image analysis. *Nat. Methods* **2012**, *9*, 671.

(24) Morrish, A. H. *The Physical Principles of Magnetism;* John Wiley & Sons: New York, 1965.

(25) Wildeboer, R. R.; Southern, P.; Pankhurst, Q. A. On the reliable measurement of specific absorption rates and intrinsic loss parameters in magnetic hyperthermia materials. *J. Phys. D: Appl. Phys.* **2014**, *47*, 495003.

(26) Psimadas, D.; Bouziotis, P.; Georgoulias, P.; Valotassiou, V.; Tsotakos, T.; Loudos, G. Radiolabeling approaches of nanoparticles with ^{99m}Tc. *Contrast Media Mol. Imaging* **2013**, *8*, 333−339.

(27) Manjunatha, H. C.; Rudraswamy, B. Exposure of bremsstrahlung from beta-emitting therapeutic radionuclides. *Radiat. Meas.* **2009**, *44*, 206−210.

(28) Caruntu, D.; Caruntu, G.; O'Connor, C. J. Magnetic properties of variable-sized Fe_3O_4 nanoparticles synthesized from non-aqueous homogeneous solutions of polyols. *J. Phys. D: Appl. Phys.* **2007**, *40*, 5801−5809.

(29) Dojčinović, B. P.; Jančar, B.; Bessais, L.; Kremenović, A. S.; Jović-Jovičić, N. P.; Banković, P. T.; Stanković, D. M.; Ognjanović, M.; Antić, B. Differently shaped nanocrystalline $(Fe,Y)_3O_4$ and its adsorption efficiency toward inorganic arsenic species. *Nanotechnology* **2019**, *30*, 475702.

(30) Gavilán, H.; Sánchez, E. H.; Brollo, M. E. F.; Asín, L.; Moerner, K. K.; Frandsen, C.; Lázaro, F. J.; Serna, C. J.; Veintemillas-Verdaguer, S.; Morales, M. P.; Gutiérrez, L. Formation Mechanism of Maghemite

Nanoflowers Synthesized by a Polyol-Mediated Process. *ACS Omega* **2017**, *2*, 7172−7184.
(31) Bouziotis, P.; Psimadas, D.; Tsotakos, T.; Stamopoulos, D.; Tsoukalas, C. Radiolabeled iron oxide nanoparticles as dual-modality SPECT/MRI and PET/MRI agents. *Curr. Top. Med. Chem.* **2013**, *12*, 2694−2702.
(32) Radović, M.; Calatayud, M. P.; Goya, G. F.; Ibarra, M. R.; Antić, B.; Spasojević, V.; Nikolić, N.; Janković, D.; Mirković, M.; Vranješ-Đurić, S. Preparation and in vivo evaluation of multifunctional 90Y□labeled magnetic nanoparticles designed for cancer therapy. *J. Biomed. Mater. Res., Part A* **2015**, *103*, 126−134.
(33) Monteiro, L. O. F.; Fernandes, R. S.; Castro, L. C.; Cardoso, V. N.; Oliveira, M. C.; Townsend, D. M.; Ferretti, A.; Rubello, D.; Leite, E. A.; de Barros, A. L. B. Technetium-99m radiolabeled paclitaxel as an imaging probe for breast cancer in vivo. *Biomed. Pharmacother.* **2017**, *89*, 146−151.
(34) Comes Franchini, M.; Pucci, A.; Locatelli, E.; Naddaka, M.; Milani; Passoni, L.; Matteoli, M.; Llop, J.; Reese, T.; Israel, L. L.; Lellouche, J. P.; Gil, L.; Gomez-Vallejo, V. Biocompatible nanocomposite for PET/MRI hybrid imaging. *Int. J. Nanomed.* **2012**, *7*, 6021.
(35) Tang, C.; Edelstein, J.; Mikitsh, J. L.; Xiao, E.; Hemphill, A. H.; Pagels, R.; Chacko, A. M.; Prud'homme, R. Biodistribution and fate of core-labeled ^{125}I polymeric nanocarriers prepared by Flash Nano-Precipitation (FNP). *J. Mater. Chem. B* **2016**, *4*, 2428−2434.
(36) Wu, T. J.; Chiu, H. Y.; Yu, J.; Cautela, M. P.; Sarmento, B.; das Neves, J.; Catala, C.; Pazos-Perez, N.; Guerrini, L.; Alvarez-Puebla, R. A.; Vranješ-Đurić, S. Nanotechnologies for early diagnosis, in situ disease monitoring, and prevention. In *Nanotechnologies in preventive and regenerative medicine;* Elsevier, 2018; pp 1−92. DOI: 10.1016/b978-0-323-48063-5.00001-0.
(37) Brezovich, I. A. Low frequency hyperthermia: capacitive and ferromagnetic thermoseed methods. *Medical physics monograph* **1988**, *16*, 82−111.
(38) Deatsch, A. E.; Evans, B. A. Heating efficiency in magnetic nanoparticle hyperthermia. *J. Magn. Magn. Mater.* **2014**, *354*, 163−172.
(39) Hergt, R.; Dutz, S.; Müller, R.; Zeisberger, M. Magnetic particle hyperthermia: nanoparticle magnetism and materials development for cancer therapy. *J. Phys.: Condens. Matter* **2006**, *18*, S2919.
(40) Jang, J. T.; Nah, H.; Lee, J. H.; Moon, S. H.; Kim, M. G.; Cheon, J. Critical enhancements of MRI contrast and hyperthermic effects by dopant-controlled magnetic nanoparticles. *Angew. Chem., Int. Ed.* **2009**, *48*, 1234−1238.
(41) Jang, J. T.; Lee, J.; Seon, J.; Ju, E.; Kim, M.; Kim, Y. I.; Kim, M. G.; Takemura, Y.; Arbab, A. S.; Kang, K. W.; Park, K. H.; Paek, S. H.; Bae, S. Giant Magnetic Heat Induction of Magnesium-Doped γ-Fe_2O_3 Superparamagnetic Nanoparticles for Completely Killing Tumors. *Adv. Mater.* **2018**, *30*, 1704362.
(42) Niculaes, D.; Lak, A.; Anyfantis, G. C.; Marras, S.; Laslett, O.; Avugadda, S. K.; Cassani, M.; Serantes, D.; Hovorka, O.; Chantrell, R.; Pellegrino, T. Asymmetric Assembling of Iron Oxide Nanocubes for Improving Magnetic Hyperthermia Performance. *ACS Nano* **2017**, *11*, 12121−12133.
(43) Bender, P.; Fock, J.; Frandsen, C.; Hansen, M. F.; Balceris, C.; Ludwig, F.; Posth, O.; Wetterskog, E.; Bogart, L. K.; Southern, P.; Szczerba, W.; Zeng, L.; Witte, K.; Grüttner, C.; Westphal, F.; Honecker, D.; González-Alonso, D.; Fernández Barquín, L.; Johansson, C. Relating Magnetic Properties and High Hyperthermia Performance of Iron Oxide Nanoflowers. *J. Phys. Chem. C* **2018**, *122*, 3068−3077.
(44) Pradhan, P.; Giri, J.; Samanta, G.; Sarma, H. D.; Mishra, K. P.; Bellare, J.; Banerjee, R.; Bahadur, D. Comparative evaluation of heating ability and biocompatibility of different ferrite-based magnetic fluids for hyperthermia application. *J. Biomed. Mater. Res., Part B* **2007**, *81B*, 12−22.
(45) Gonzales-Weimuller, M.; Zeisberger, M.; Krishnan, K. M. Size-dependant heating rates of iron oxide nanoparticles for magnetic fluid hyperthermia. *J. Magn. Magn. Mater.* **2009**, *321*, 1947−1950.
(46) Lee, J. H.; Jang, J. T.; Choi, J. S.; Moon, S. H.; Noh, S.-H.; Kim, J. W.; Kim, J. G.; Kim, I. S.; Park, K. I.; Cheon, J. Exchange-coupled magnetic nanoparticles for efficient heat induction. *Nat. Nanotechnol.* **2011**, *6*, 418−422.
(47) Wydra, R. J.; Rychahou, P. G.; Evers, B. M.; Anderson, K. W.; Dziubla, T. D.; Hilt, J. Z. The role of ROS generation from magnetic nanoparticles in an alternating magnetic field on cytotoxicity. *Acta Biomater.* **2015**, *25*, 284−290.
(48) Hardiansyah, A.; Huang, L. Y.; Yang, M. C.; Liu, T. Y.; Tsai, S. C.; Yang, C. Y.; Kuo, C. Y.; Chan, T.-Y.; Zou, H. M.; Lian, W. N.; Lin, C. H. Magnetic liposomes for colorectal cancer cells therapy by high-frequency magnetic field treatment. *Nanoscale Res. Lett.* **2014**, *9*, 497.

DOI: 10.1021/acsami.9b16428
ACS Appl. Mater. Interfaces 2019, 11, 41109−41117